Computers & Fluids, Volume 37, Issue 7, August 2008, Pages 867-876

Large-eddy simulation of multi-component compressible turbulent flows using high resolution methods

B.Thornber * **D.Drikakis**

Fluid Mechanics and Computational Science Group, Department of Aerospace Sciences, Cranfield University, UK

D.Youngs

AWE, Aldermaston, UK

ABSTRACT

The ability of a finite volume Godunov and a semi-Lagrangian Large Eddy Simulation (LES) method to predict shock induced turbulent mixing has been examined through simulations of the half-height experiment (Holder and Barton, Proceedings of the International Workshop on the Physics of Compressible Turbulent Mixing, 2004). Very good agreement is gained in qualitative comparisons with experimental results for combined Richtmyer-Meshkov and Kelvin-Helmholtz instabilities in compressible turbulent multicomponent flows. It is shown that both numerical methods can capture the size, location and temporal growth of the main flow features. In comparing the methods, there is variability in the amount of resolved turbulent kinetic energy. The semi-Lagrangian method has constant dissipation at low Mach number, thus allowing the initially small perturbations to develop into Kelvin-Helmholtz instabilities. These are supressed at the low Mach stage in the Godunov method. However, there is excellent agreement in the final amount of fluid mixing when comparing both numerical methods at different grid resolutions

Key words: LES, ILES, turbulence, compressible, mixing
PACS: 47.27

1 INTRODUCTION

This paper focuses on the three dimensional simulation of shock induced turbulent mixing of two different gases via Kelvin-Helmholtz and Richtmyer-Meshkov (RM) type instabilities. As current computational power does not allow Direct Numerical Simulation of such complex flows, Large-eddy simulation (LES) is emerging as a viable alternative in flows of industrial interest where the time dependent behaviour of the flow must be resolved. Conventional LES [1], where an explicit subgrid model is added to the averaged Navier Stokes equations, has been employed successfully in many prototype flows, however it is known to provide excessive dissipation in flows where the growth of an initially small perturbation to fully turbulent flow must be resolved [2,3].

* Corresponding author. Tel.:+44 1234 750111 (Ext 5141) Fax: +44 1234 758207
Email address: b.j.r.thornber@cranfield.ac.uk (B.Thornber).

It has been recognised that some numerical schemes gain good results in complex flows without the explicit addition of a subgrid model [2,4,1]. This approach is termed Implicit Large-eddy Simulation, or ILES. Excellent results have been gained in ILES simulation of flows as varied as Rayleigh-Taylor and Richtmyer Meshkov mixing [5,6], Free jets [7], convection of plumes, channel flow [7], cavity flow [8], geophysical flows [9] and decaying turbulence [8,10–12].

This agreement stems from the understanding that the subgrid stresses arise from the Finite Volume (FV) averaging process itself. A Taylor series expansion of the subgrid terms (as carried out for Approximate Deconvolution methods, see [12,13] for example) assuming a top hat filter in physical space yields the same series as the conversion of a FV averaged quantity to a cell centred exact quantity. This means that for well constructed FV schemes there is a distinct link between the interpolation method and subgrid stresses - which may or may not be ascribed to turbulence. Thus, for example, a third order FV scheme contains inherently a second order accurate expansion of the exact subgrid stress tensor. Typically, FV schemes are constructed along one dimensional lines in computational space thus there are certain three dimensional terms which are missing in the one dimensional stencils, meaning that they are not an exact match to a second order expansion of the subgrid stress tensor. It is additionally recognised that MUSCL-based methods typically give a dissipative spectra at high wavenumbers as a consequence of flow regularisation for reasons of numerical stability [14], however the growth rate of the integral length scales and dissipation rate of turbulent kinetic energy can be captured reasonably (See references in the previous paragraph).

Thus this paper investigates comparatively the ability of a finite volume Godunov scheme and a semi-lagrangian finite difference method to simulate a compressible mixing experiment involving shock waves, strong shear layers, and initially small instabilities (relative to the grid dimension). The organisation is as follows. In Section 2 the mixing experiment is described. Next, Section 3 discusses the two numerical methods employed in this paper, including the multicomponent models and modelling assumptions inherent in representing the experimental setup. Section 4 compares the qualitative experimental results with the results from both numerical methods. Additionally, issues of grid convergence with respect to turbulent kinetic energy and mixing are discussed. Finally conclusions are drawn in Section 5

2 EXPERIMENTAL CONFIGURATION

Fig. 1 shows a schematic of the half-height experiment (See [15] for the full details). A Mach 1.26 shock wave in air passes through a block of SF_6 initially held in place by a microfilm membrane, and seeded with olive oil droplets. A system consisting of a pulsed laser sheet and high speed cameras was used to produce images for validation of multi-component compressible methods for turbulent mixing problems. These are used for comparison here as no quantitative data was produced from the experiments. The shock passes more slowly through the SF_6 than through the air above the block which creates a Kelvin-Helmholtz instability at the upper interface, with RM instabilities at the two vertical interfaces. Transition to turbulence occurs rapidly in the spiral of the large primary vortex promoting mixing dominated by turbulent transport of the individual gases. The shock reflects off the end wall of the tube, and passes through the turbulent mixing zone which increases the mixing rate and produces a complex set of reflected, refracted and transmitted shocks.

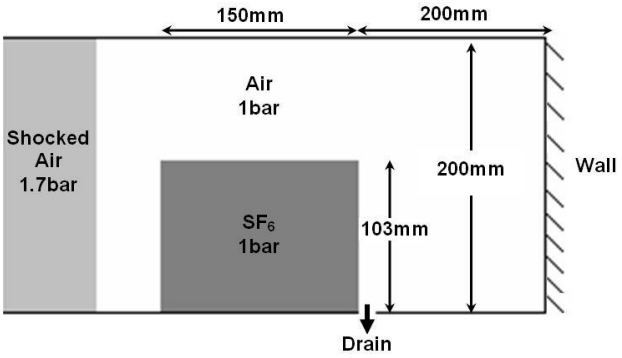

Fig. 1. Schematic of the half-height experiment, note that the shock tube is 100mm deep

3 COMPUTATIONAL APPROACH

3.1 Numerical Methods

For the experiment under consideration, the form of the initial perturbations can affect significantly the growth of the resulting mixing layer, so the initial perturbations should be allowed to grow without being dissipated (or enhanced) by the numerical method. Additionally, the monotonicity of the various gas properties must be maintained, and the shocks captured accurately. With an experimental Reynolds number on the order of 3×10^8 at $4ms$, the Kolmogorov lengthscale in the experiment would be significantly smaller than the mesh size used in this study. With this in mind is assumed that viscous effects are negligible on the scales resolved by the grid, and so the governing equations chosen are the Euler equations plus one or two additional equations for the multi-component model. At the pressures and temperatures considered, both SF_6 and air are approximately well by the ideal gas equation of state, and are miscible.

Two numerical methods have been selected which differ significantly in numerical approach and choice of multicomponent equations. The first numerical methods is implemented within a code called 'CNS3D' and is a FV Godunov method using a characteristics based Riemann solver [16]. The multi-component model is based on the conservation of total enthalpy within the fluid mixture [17]. This requires the computation of two additional equations in conservation form

$$\frac{\partial}{\partial t}\left(\frac{\rho\chi}{M}\right) + \frac{\partial}{\partial x_i}\left(\frac{\rho u_i \chi}{M}\right) = 0, \tag{1}$$

$$\frac{\partial}{\partial t}\left(\frac{\rho}{M}\right) + \frac{\partial}{\partial x_i}\left(\frac{\rho u_i}{M}\right) = 0 \tag{2}$$

where M is the molecular mass of the mixture, and the variable χ is defined for a perfect gas as,

$$\chi = \frac{\gamma}{\gamma - 1}. \tag{3}$$

To derive an approximate Riemann solver, dimensional splitting is applied to the fully coupled system of equations. The characteristic flux employs the Riemann invariants of the system which are solved to give estimates of the interface values in terms of an integral change of the conserved variables along the characteristic lines. These integral changes are replaced by the jumps along the characteristic lines thus allowing solution of the initially non-linear problem. Higher order accuracy is achieved through van Leer's MUSCL limiting technique [18] where the left and right extrapolated states are defined as

$$U^L_{i+1/2} = U_i + \frac{1}{2}\phi\left(r^L\right)\left(U_i - U_{i-1}\right), \tag{4}$$

$$U^R_{i+1/2} = U_{i+1} - \frac{1}{2}\phi\left(r^R\right)\left(U_{i+2} - U_{i+1}\right), \tag{5}$$

where U is the vector of cell averaged conserved variables,and

$$r^L_i = \frac{U_{i+1} - U_i}{U_i - U_{i-1}}, \tag{6}$$

$$r^R_i = \frac{U_{i+1} - U_i}{U_{i+2} - U_{i+1}}. \tag{7}$$

Within this paper, the second order van Leer limiter is used,

$$\phi_{VL} = \frac{2r}{1+r}. \tag{8}$$

Time advancement is achieved using the 3rd order Runge Kutta method [19]

$$U_i^1 = U_i^n + \frac{1}{2}\frac{\delta t}{\delta x} f\left(U_i^n\right), \tag{9}$$

$$U_i^2 = U_i^n + \frac{1}{2}\frac{\delta t}{\delta x}[f\left(U_i^1\right)], \tag{10}$$

$$U_i^{n+1} = \frac{1}{3}\left(2U_i^2 + U_i^n + \frac{\delta t}{\delta x}[f\left(U_i^2\right) + f\left(U_i^1\right)]\right). \tag{11}$$

TURMOIL3D uses a Lagrange- remap method [20]. For turbulent mixing problems a mass fraction advection equation is used for gas mixtures [6].The Lagrange phase calculates the changes in velocity and internal energy due to the pressure field. A staggered mesh is used with velocity components defined at cell corners and with density, mass fraction and internal energy defined at cell centres. A finite difference approximation is used which is second order accurate in space and time and conserves total energy. Quadratic artificial viscous pressure, q, is used to provide the dissipation due to shocks. There are oscillations behind shocks. Hence the treatment of shocks is not as good as in second-order Godunov methods. However, the method does have one very useful property: the irreversible dissipation of kinetic energy, $-q\nabla\cdot\mathbf{u}$, is negligible for low Mach number, near incompressible flow. All three spatial directions are calculated simultaneously in the Lagrange phase.

The remap phase calculates advective fluxes and may be regarded as a remap of the configuration at the end of the Lagrangian motion, back to the original mesh. X, Y and Z advection are calculated in separate one-dimensional sweeps using a third order monotonic method based on the work of van Leer. The order of the sweeps is reversed every time step. Several Lagrange steps may be performed per remap step and this significantly increases the efficiency of low Mach number calculations. The method gives exact monotonic behaviour i.e. fluid variables at the end of the remap phase lie with the range of neighbouring values at the end of the Lagrange phase. The remap phase conserves mass, internal energy and momentum. However, kinetic energy is dissipated. The loss of kinetic energy may be quantified precisely as a function of position by the simple algebraic technique of DeBar [21] and may be added on to the internal energy to recover total energy conservation. This technique may also be used to quantify the sub-grid dissipation which occurs where there are steep velocity gradients and is negligible in regions of smooth flow. The resulting dissipation is comparable to that obtained with an explicit sub-grid-scale model.

For shock tube applications the x-direction mesh (the direction of shock propagation moves) with the mean x-velocity i.e. a semi-Lagrangian calculation is performed. This is achieved by a simple change to the remap phase - remap back to a displaced mesh.

The major difference in the two approaches is in the nature of the dissipation of kinetic energy by the numerical schemes at low Mach. It is well known that Godunov schemes suffer from poor accuracy at low Mach numbers due to excessively dissipative behaviour, causing a steep increase in dissipation in low Mach flows [22]. However, the semi-lagrangian method maintains constant dissipation at low Mach, allowing low Mach perturbations or instabilities to develop more freely. Both method should capture the large scale flow accurately as the Mach number of the dominant flow structures within the experiment is 0.9, however the appearance of smaller structures depends

on the resolution of instabilities, which can occur at Mach numbers much lower than the mean flow Mach number.

3.2 Initialisation and Modelling Assumptions

Several modelling assumptions are made to initialise the numerical simulation. It is assumed that the transport and mixing of SF_6 is determined only by turbulent motion, and that the Reynolds number is high enough to neglect the viscous terms in the governing equations. The co-ordinate system chosen has the x direction aligned with the initial direction of shock propagation, z in the vertical direction, and y in the homogeneous direction. The point $(0, 0, 0)$ is located at the bottom left hand interface between the SF_6 block and air. The total domain size (initially in the case of the semi-Lagrangian method) extends from -0.45m to 0.35m in x, and takes the shock tube dimensions in the other two directions.

The boundary conditions are free slip walls in the z direction, with supersonic inlet and free slip wall in the left and right x direction. The y direction boundary conditions are periodic. TURMOIL3D employs a one dimensional domain instead of the inlet condition to allow waves to exit the domain without reflection. Finally, the drain hole was not modelled in TURMOIL3D as it was considered not to have a large effect on the turbulent mixing of the primary vortex. Two-dimensional calculations of the half-height experiment [23] have shown that modelling the drain hole gives improved agreement with experiment. The effects of the drain hole were also investigated using CNS3D, modelling the hole as a one dimensional slat in the base of the shock tube, using a one dimensional version of the CNS3D solver. This was chosen instead of traditional boundary conditions such as specifying the pressure, or extrapolation which are not appropriate in this case. The drain hole is located between $0.153\text{m} < x < 0.16\text{m}$ and $0.05\text{m} < y < 0.95\text{m}$.

The initial perturbation imparted on the vertical gas interface by the membrane was modelled as a summation of random modes with RMS amplitude of 0.1mm at wavelengths between 5mm to 50mm satisfying a power spectra proportional to the wavenumber of the mode.

The object of the simulations is to compare both numerical methods with experiment, and also with each other. Thus both methods were run at the same cross-sectional mesh resolutions of $y \times z = 160 \times 320$ with CNS3D having 600 cells in the x direction, and TURMOIL3D 640 cells. The aim was to maintain the same cross-sectional resolution with both numerical methods, whereas the x-direction mesh cannot be the same as the size of the domain in the x-direction changes during the course of the simulation when using the semi-lagrangian scheme. The effects of grid size were investigated using a coarse resolution grid of $300 \times 80 \times 160$ with CNS3D, and a fine resolution grid of $1280 \times 320 \times 640$ with TURMOIL3D. The density of SF_6 and air were 6.34kg/m^3 and 1.153kg/m^3, and the Ratios of specific heats 1.076 and 1.4 respectively.

4 Results and Discussion

4.1 Comparison with Experiment

Fig. 2 compares the experimental images with plane slices of SF_6 density taken from computational results. The vertical reference line on the experimental images is at $x = 0.15$m. For the first two time steps the numerical methods and the experiment give very similar results. The only disagreement is at the primary vortex which remains more coherent in the simulations than in reality.

At 1ms the first differences between the numerical methods occur as instabilities in the primary

(a) 0.20ms

(b) 0.37ms

(c) 1ms

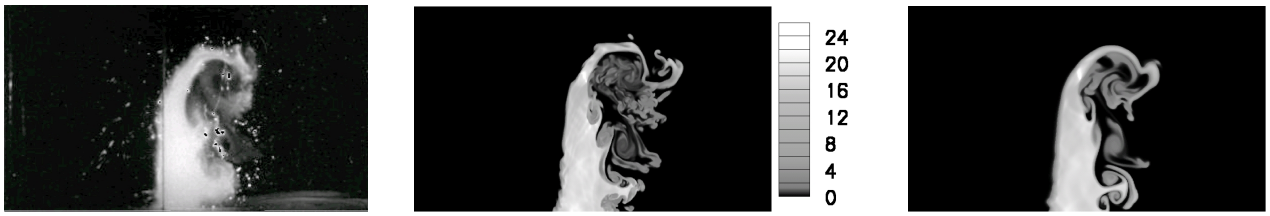

(d) 2ms

(e) 3ms

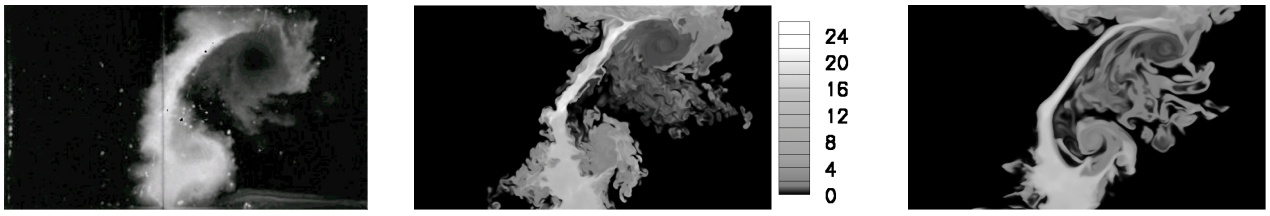

(f) 4ms

Fig. 2. Comparison of experimental images (left,©British Crown Copyright 2006/MOD) and SF_6 density (kg/m^3) for TURMOIL3D (centre) and CNS3D (right) using the grid of cross-section of 160×320

vortex in TURMOIL3D, which are not present in CNS3D. At this point the angled shock converges near the wall causing high pressures, densities and velocities, leading to the 'bump' visible at the right hand interface. The incident shock, reflecting from the end wall, passes through this bump triggering an RM instability producing the large mushroom shaped injection of heavy gas.

At 2ms both methods show good agreement in terms of the position of the primary vortex, and the presence of significant turbulent mixing in the vortex core. This mixing occurs at a smaller scale in TURMOIL3D than with CNS3D. The mushroom shaped injection of heavy gas is orientated upwards in both simulations, however in the experiment this remained horizontal. This discrepancy is due to not modelling the drain hole shown in Fig. 1, as will be discussed later in this section.

The primary vortex reaches the top of the shock tube at 3ms in both experiment and simulations, indicating that the growth of the length scales present in the experiment are captured well. At 4ms the thin line connecting the remains of the block with the primary vortex is less mixed in the simulation than in the experiment. In the experiment this mixing is caused by an RM instability at a scale below that which is captured in the moderate resolution simulations. Fig. 3 shows volume fraction iso-surfaces at 3ms, illustrating the highly turbulent nature of the flow.

The SF_6 density at 3ms and 4ms taken from the simulation with the drain hole included are shown in Fig. 4. The drain hole causes a high speed jet flow exiting the shock tube which significantly effects the flow geometry in the region near to the hole at late times. As can be seen, the mushroom shape is now close to horizontal as shown in the experimental images.

The experimental images in Fig. 2 are more diffuse that the plane slices taken from the computations. Fig. 5 shows results from the medium res-

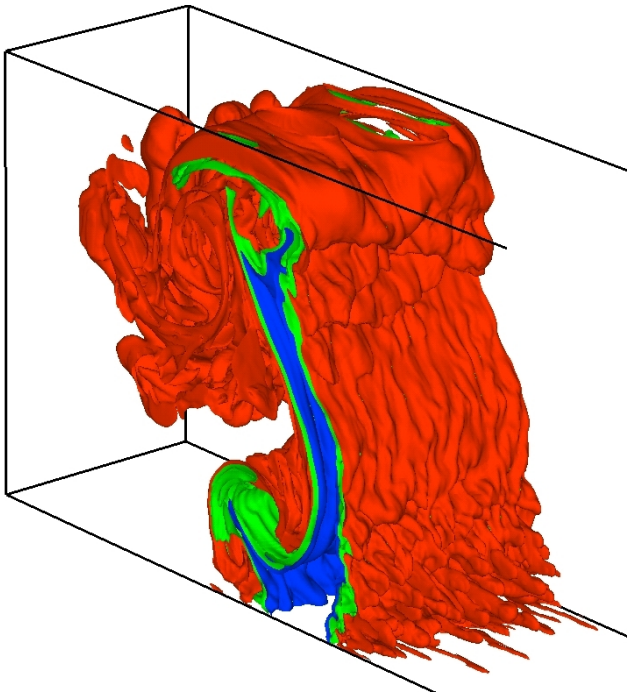

Fig. 3. Iso-surfaces of 1%, 50% and 99% volume fraction of air from the $600 \times 160 \times 320$ resolution CNS3D simulation

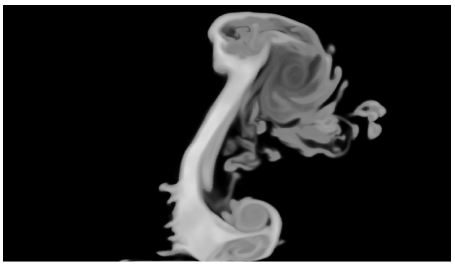

(a) 3ms

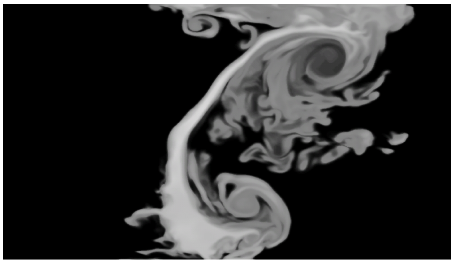

(b) 4ms

Fig. 4. Plane slices of SF_6 density computed on a $600 \times 160 \times 320$ grid using CNS3D including the drain hole

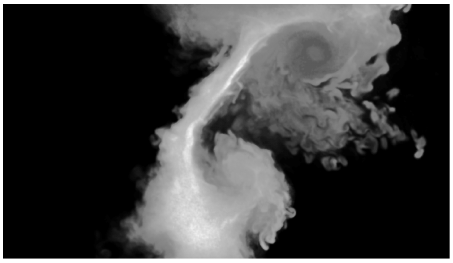

Fig. 5. TURMOIL3D results on the $640 \times 160 \times 320$ at 4ms post-processed with a Monte-Carlo software to compensate for scattering effects

olution TURMOIL3D simulation at 4ms which have been post-processed using a Monte-Carlo approach [24]. The laser sheet produces an image by Mie scattering. The seeding level is high enough for multiple scattering to be significant and when this is taken into account a more diffuse image is obtained, in better qualitative agreement with experiment.

The position of the shock wave and SF_6 block have been extracted from the experimental data and a comparison of these can be seen in Fig. 6. The agreement of the position of the deformed SF_6 block is excellent, especially at the left and upper interface. There is only a small discrepancy in the angle of the refracted shock, which has a less steep angle in the experiment due to initial diffusive mixing at the upper SF_6/air boundary. This figure also demonstrates that CNS3D with the THCM gas mixture model captures the shock without any oscillations. There are some oscillations behind the shock in the TURMOIL3D solution, apparent at 0.37ms.

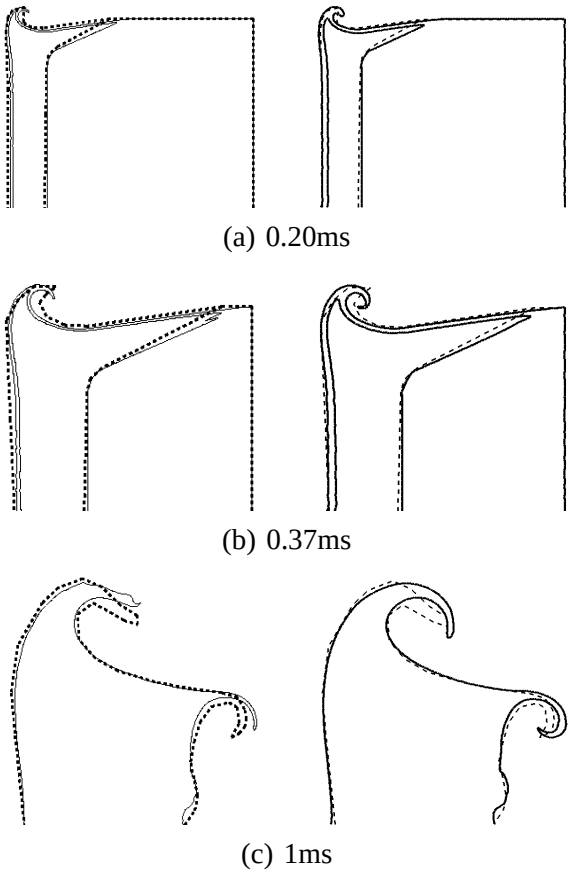

(a) 0.20ms

(b) 0.37ms

(c) 1ms

Fig. 6. Comparison of experimental shock and SF_6 positions (dashed line) and numerical results (solid line) for TURMOIL3D (Left) and CNS3D (right) using the grid of cross-section of 160×320

4.2 Turbulent Mixing and Kinetic Energy

This section compares spatially averaged turbulent kinetic energy and levels of mixing at different mesh resolutions and using different schemes. Fig. 7 shows the y-averaged SF_6 density at time 4ms. The fine and moderate resolution TURMOIL3D results appear almost identical, and CNS3D differs only slightly in the position of the mushroom shaped feature and has less fine scale features.

Fig. 8 presents plane averaged mixing $< f_1 >< f_2 >$, and Fig. 9 the quantity $< f_1 f_2 >$, which is a measure of the amount of molecular mixing in the primary vortex. f_1 is the volume fraction of Air and f_2 that of SF_6. An improvement can be seen in the level of mixing in the 'thin strip' at high resolution, however there there is excellent agreement in the magnitude and location of the peaks of molecular mixing in all simulations. Interestingly, the extent of the mixing in the primary vortex ($0.17 < x < 0.28$) does not change significantly with a quadrupling in mesh resolution, indicating that CNS3D is compensating for the lack of resolution by adding some subgrid

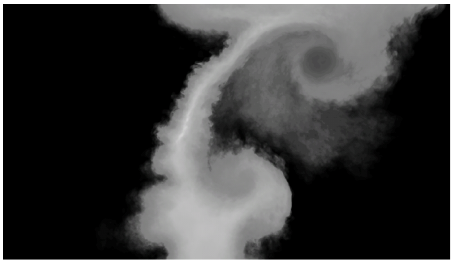

(a) TURMOIL3D $1280 \times 320 \times 640$

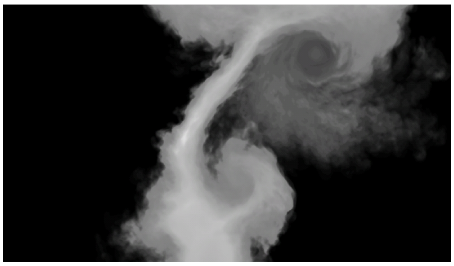

(b) TURMOIL3D $640 \times 160 \times 320$

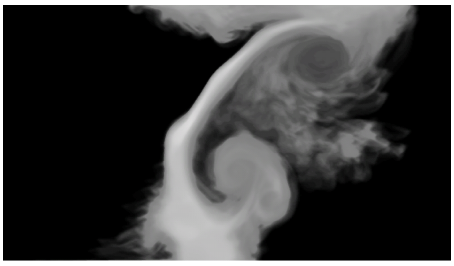

(c) CNS3D $600 \times 160 \times 320$

Fig. 7. Line average SF_6 density at 4ms

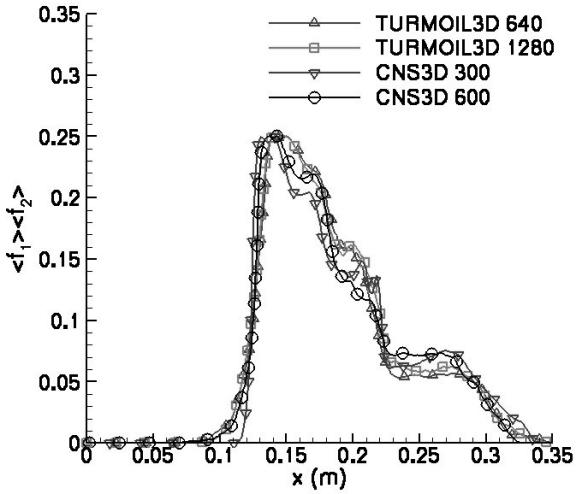

Fig. 8. Comparison of $< f_1 >< f_2 >$ at 4ms

dissipation in a physical manner.

The turbulent kinetic energy per metre is defined as

$$KE = \frac{1}{2} \int \rho K dy dz, \tag{12}$$

$$K = (u - \tilde{u})^2 + v^2 + (w - \tilde{w})^2, \tag{13}$$

where the tilde quantities are Favre mass-weighted mean velocities in the homogeneous direction

$$\tilde{u} = \frac{\overline{\rho u}}{\bar{\rho}}, \qquad \tilde{w} = \frac{\overline{\rho w}}{\bar{\rho}}, \tag{14}$$

and $\bar{(.)}$ indicates a line averaged quantity in the periodic y direction. This is plotted in Fig. 10 for t=4ms. There are two clear locations where the turbulent kinetic energy peaks, the first is at $x = 0.21$ which corresponds to the mushroom shape and the back of the primary vortex, and the maximum at $x = 0.25$ corresponding to the primary vortex core and the turbulent vortices directly below that core. Comparing the moderate and fine resolutions, the magnitude of the maximum kinetic energy agrees to within 13%, and the position is nearly identical in all higher resolution simulations. The second order MUSCL scheme has less turbulent kinetic energy when compared to the Lagrangian scheme in the region $0.1 < x < 0.2$, where the local integral length scale is smaller than at the primary vortex.

Finally, the evolution of total resolved turbulent kinetic energy (TKE) as a function of time is shown in Fig. 11. Initially, the TKE is higher at high resolution as the turbulent kinetic energy is concentrated at small scales. As the instabilities grow, the turbulent kinetic energy is seen at a larger scale and thus the TKE in the moderate resolution simulation begins to rise. The peak of the total turbulent kinetic energy occurs at t=2.5ms, which can be attributed to the development of the initial Kelvin-Helmholtz shear layer into a single turbulent vortex. However, after

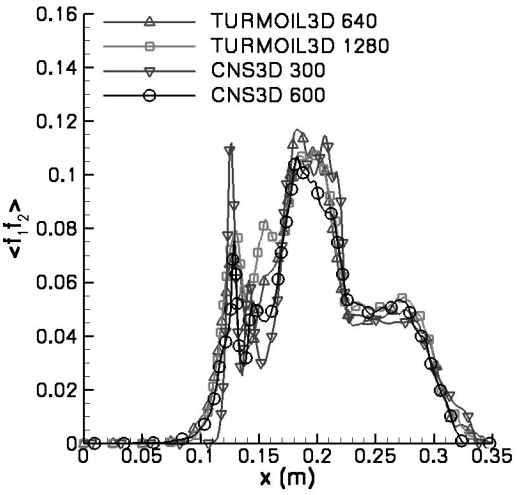

Fig. 9. Comparison of $< f_1 f_2 >$ at 4ms

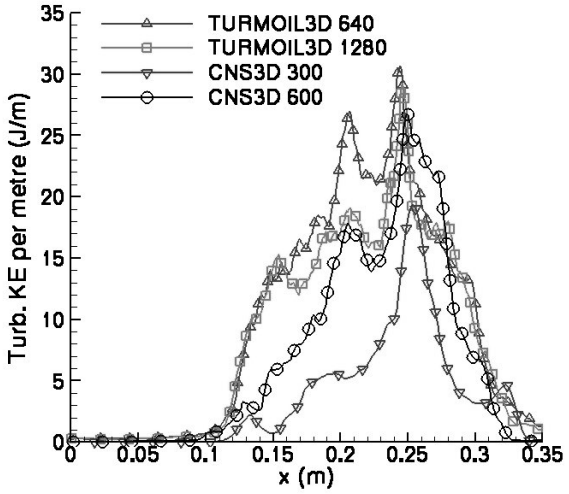

Fig. 10. Comparison of turbulent kinetic energy per metre at 4ms

2.5ms the fine resolution TURMOIL3D simulation dissipates the kinetic energy more rapidly. The higher TKE in the semi-lagrangian simulations can be attributed to the behaviour of the kinetic energy dissipation within the numerical scheme. As mentioned in Section 3, the Godunov scheme dissipates more heavily at lower Mach, whereas the semi-Lagrangian scheme does not. In the semi-Lagrangian methods, initially small perturbations on the SF_6 interface are allowed to grow with less dissipation, and these are the source of Kelvin-Helmholtz type instabilities triggering fine scale turbulent features. However,

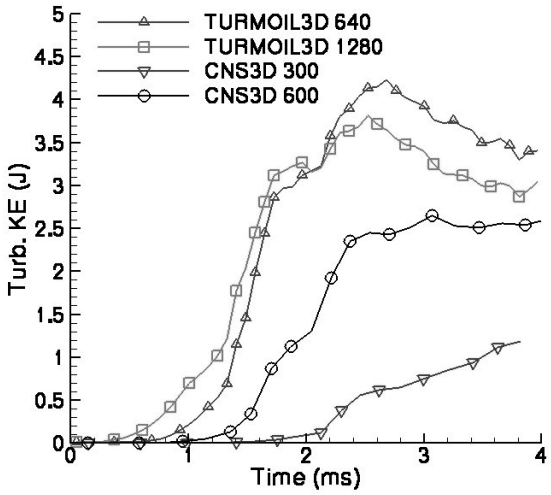

Fig. 11. Comparison of total resolved turbulent kinetic energy variation with time, where time is measured from the passage of the shock through the first interface

these also remove energy from the large scales, thus the resolved TKE in the semi-Lagrangian simulations decays more rapidly than the Godunov scheme. The coarse simulation captures less than 25% of the TKE in the finer simulations, thus it is interesting that the plane averaged mixing parameters in Fig. 8 and 9 have such a reasonable agreement.

5 CONCLUSIONS

This paper has compared the performance of two very different ILES methods in simulating an experiment involving complex shock induced mixing. The two methods employed were CNS3D, a FV characteristics based scheme with MUSCL variable extrapolation to achieve higher order accuracy, and TURMOIL3D, a third order semi-Lagrangian scheme.

Comparison with the half-height experiment shows excellent qualitative agreement with the available experimental data in terms of the size, location and temporal growth of the main flow features. Convergence was tested against a high

resolution simulation which gave improved mixing at the 'thin strip' between the mushroom and primary vortex features, however the mixing in the primary vortex was not affected greatly. In addition, the shock positions are captured accurately demonstrating the effectiveness of the multicomponent models. It was demonstrated that the discrepancy in the position of the mushroom shaped feature was due to not modelling the drain hole in the initial simulations.

The two methods are in excellent agreement for overall degree of plane averaged mixing and molecular mixing at all resolutions. TURMOIL3D allows more fine scale turbulent mixing than CNS3D with van Leer limiting, which is reflected in the higher total turbulent kinetic energy. This is because the semi-lagrangian method maintains constant dissipation at low Mach, thus allowing the growth of initially low Mach number perturbations, which is not the case for the Godunov method. Despite this, both numerical methods at moderate resolution predict the x-location of the maxima of resolved turbulent kinetic energy to within 3mm of the fine resolution simulation, and the magnitude to within 13%. CNS3D with the THCM model captures shock waves better than TURMOIL3D.

Future work is focusing on the development of very high order methods for compressible flows, and on a complete characterisation of the dissipative properties of FV numerical methods. It is hoped that this will improve results for FV schemes in areas of strong shear such as the Kelvin-Helmholtz instability reported in this paper, allowing accurate simulations at lower resolutions.

6 ACKNOWLEDGEMENTS

The authors would like to acknowledge financial support through an EPSRC-AWE PhD CASE award and an EPSRC-MoD (Dstl, AWE) research grant (EP/C515153 & JGS 971). They would also like to acknowledge stimulating discussions with Robin Williams, Anthony Weatherhead at AWE, and Evgeniy Shapiro at Cranfield University.

The computations for this paper were carried out on the Cranfield-Cambridge High Performance Computing Facility, and the Blue Oak at AWE.

BIBLIOGRAPHY

[1] P. Sagaut, Large Eddy Simulation for Incompressible Flows, Springer Verlag, 2001.

[2] M. Lesieur, O. Metais, New trends in large-eddy simulations of turbulence, Annu. Rev. Fluid Mech. 28 (1996) 45–82.

[3] S. Pope, Turbulent Flows, Cambridge University Press, 2000.

[4] D.Drikakis, Advances in turbulent flow computations using high-resolution methods, Prog. Aerosp. Sci. 39 (2003) 405–424.

[5] D. Youngs, Numerical simulation of mixing by rayleigh-taylor and richtmyer-meshkov instabilities, Laser Part. Beams 12 (1994) 725–750.

[6] D. Youngs, Three-dimensional numerical simulation of turbulent mixing by rayleigh-taylor instability, Phys. Fluids A 3 (5) (1991) 1312–1320.

[7] F. Grinstein, C. Fureby, Recent progress on miles for high reynolds number flows, J. Fluid Eng.-T. ASME 848 (2002) 848–861.

[8] M. Hahn, D. Drikakis, Large eddy simulation of compressible turbulence using high-resolution method, Int. J. Numer. Meth. Fl. 49 (2005) 971–977.

[9] L. Margolin, P. Smolarkiewicz, Z. Sorbjan, Large-eddy simulations of convective boundary layers using nonoscillatory differencing, Physica D 133 (1999) 390–397.

[10] D. Porter, P. Woodward, A. Pouquet, Inertial range structures in decaying compressible turbulent flows, Phys. Fluids 10 (1) (1998) 237–245.

[11] C. Fureby, F. Grinstein, Large eddy simulation of high-reynolds-number free and wall-bounded flows, J. Comput. Phys. 181 (2002) 68–97.

[12] L. Margolin, W. Rider, F. Grinstein, Modeling turbulent flow with implicit les, J. Turbul. 7 (15) (2006) 1–27.

[13] S. Stolz, N. Adams, An approximate deconvolution procedure for large-eddy simulation, Phys. Fluids 11 (7) (1999) 1699–1701.

[14] E. Garnier, M. Mossi, P. Sagaut, P. Comte, M. Deville, On the use of shock-capturing schemes for large-eddy simulation, J. Comput. Phys. 153 (1999) 273–311.

[15] D. Holder, C. Barton, Shock tube richtmyer-meshkov experiments: inverse chevron and half height, in: Proceedings of the 9th IWPCTM, 2004.

[16] A. Eberle, Characteristic flux averaging approach to the solution of euler's equations, Tech. rep., VKI Lecture Series (1987).

[17] S. Wang, M. Anderson, J. Oakley, R. Corradini, M.L.and Bonazza, A thermodynamically consistent and fully conservative treatment of contact discontinuities for compressible multi-component flows, J. Comput. Phys. 195 (2004) 528–559.

[18] B. van Leer, Towards the ultimate conservative difference scheme.iv. a new approach to numerical convection, J. Comput. Phys. 23 (1977) 276–299.

[19] R. Spiteri, S. Ruuth, A class of optimal high-order strong-stability preserving time discretization methods, SIAM J. Sci. Comput. 4 (2) (2002) 469–491.

[20] D. Youngs, Time-dependent multimaterial flow with large fluid distortion, in: Numerical Methods for Fluid Dynamics, Academic Press, 1982, pp. 273–285.

[21] R. Debar, A methodin two-d eulerian hydrodynamics, Tech. Rep. UCID-196831, Lawrence Livermore National Laboratory (1974).

[22] G. Volpe, Performance of compressible flow codes at low mach number, AIAA J. 31 (1993) 49–56.

[23] K. Bates, N. Nikiforakis, D. Holder, Richtmyer-meshkov instability induced by the interaction of a shock wave with a block of sf_6, submitted to Phys. Fluids.

[24] D. Holder, A. Smith, C. Barton, D. Youngs, Shock-tube experiments on richtmyer-meshkov instability growth using an enlarged double-bump perturbation., Laser Particle Beams 23 (2003) 411–418.